GLRS-R 2-COLOUR RETROREFLECTOR TARGET DESIGN AND PREDICTED PERFORMANCE

Glenn LUND
Optical Department
AEROSPATIALE - Space & Defense Division
100 Boulevard du Midi
06322 CANNES LA BOCCA
FRANCE

ABSTRACT

This paper reports on the retroreflector ground-target design for the GLRS-R spaceborne dual-wavelength laser ranging system.

The described passive design flows down from the requirements of high station autonomy, high global FOV (up to 60° zenith angle), little or no multiple pulse returns, and adequate optical cross-section for most ranging geometries. The proposed solution makes use of 5 hollow cube-corner retroreflectors of which one points to the zenith and the remaining four are inclined from the vertical at uniform azimuthal spacings.

The need for fairly large (~ 10 cm) retroreflectors is expected (within turbulence limitations) to generate quite narrow diffraction lobes, thus placing non-trivial requirements on the vectorial accuracy of velocity aberration corrections. A good compromise solution is found by appropriately spoiling just one of the retroreflector dihedral angles from 90°, thus generating two symmetrically oriented diffraction lobes in the return beam. The required spoil angles are found to have little dependance on ground target latitude.

Various link budget analyses are presented, showing the influence of such factors as point-ahead optimisation, turbulence, ranging angle, atmospheric visibility and ground-target thermal deformations.

1. BASIC GROUND TARGET REQUIREMENTS

During the various study phases investigated during the course of the GLRS project, the Ground Target (GT) requirements established to be of most significant importance were the following :

- Choice of a multiple-retroreflector, passive target concept.
- As nearly full coverage of the sky as possible, up to local zenith angles of at least 60°.
- Avoidance of ambiguous (multiple) pulse returns.
- Adequate velocity aberration correction, in keeping with the link budget requirements.
- Adequate photon budget for sub-centimetric ranging accuracies under most clear atmospheric conditions.
- Moderate cost and high reliability.

The requirement of a *passive* GT design leads to the choice of a *multiple* fixed Retroreflector (RR) concept where full sky coverage is achieved by the summation of several contributing RR FOVs.

The inherent difficulties in this approach result firstly from the *non*-uniform reflected energy diagram of a static RR, and secondly - because of the gradual fall-off of this diagram - from the requirement of inter-RR crosstalk (i.e. multiple pulse return) avoidance.

The adopted solution must therefore achieve an acceptable compromise between somewhat conflicting requirements and the need for accurate range measurements to be achieved under *most* conditions.

In the following sections the proposed GLRS-R GT design is described, and its numerically simulated performance is illustrated as a function of several important system variables.

2. BASELINE GLRS-R TARGET CONCEPT

The baseline 5-retroreflector GT design illustrated in Fig. 1 provides a good compromise between full sky coverage, minimal FOV overlap and minimal number of RRs. The individual retroreflectors have a useful diameter of 100 mm, and will need to be of hollow construction in order to minimise thermally induced wavefront deformations. Although good thermal performance is achieved (in space applications) with small solid cube-corners, there are practical limits in *size* and *temperature excursion* beyond which

the resulting refractive-index gradients will generate unacceptable wavefront distortions.

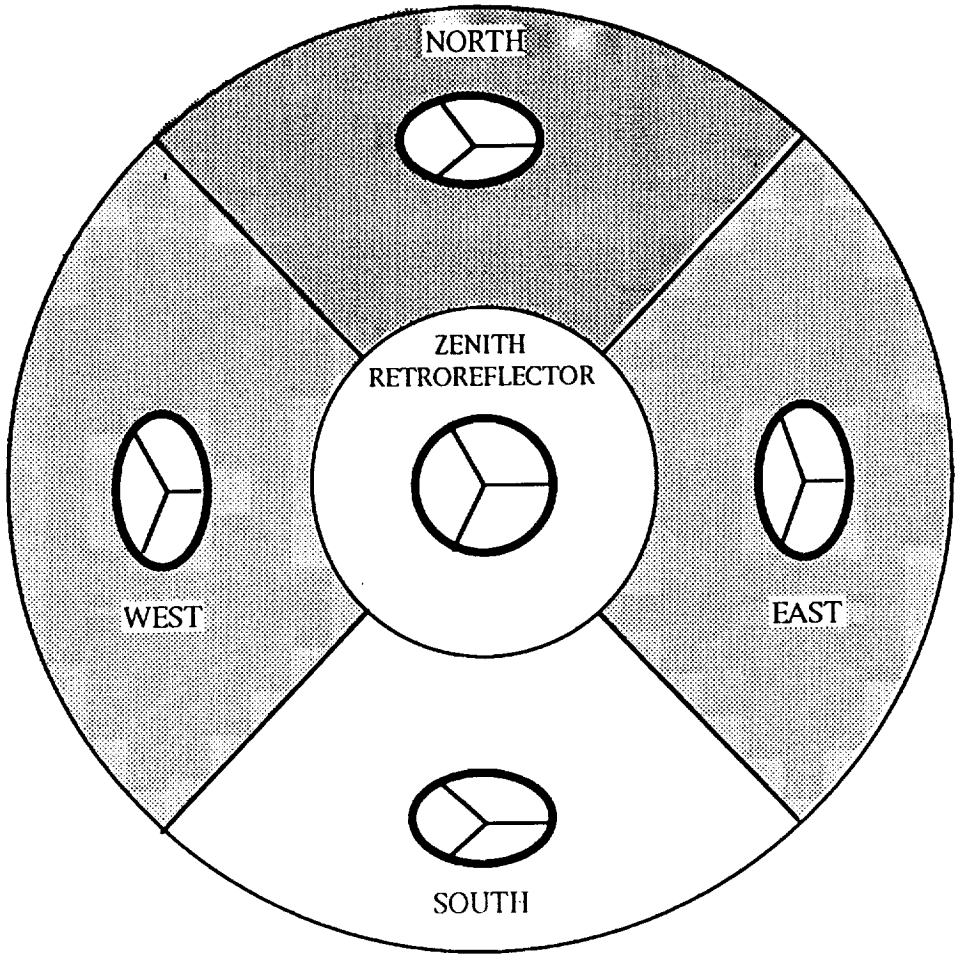

Figure 1. Proposed baseline 5 - cube corner ground-target

As shown in § 10p, thermo-mechanical effects can also lead to wavefront distortions in hollow retroreflectors, although they are expected to be an order of magnitude smaller than those induced under comparable conditions in a refractive medium. For reasons of resistance to environmental influences, the hollow reflectors will need to be covered by a protective (optical quality) window.

Preliminary thermo-mechanical analysis has shown that the GT *support structure* can be made of common materials which would give rise to reflector location stabilities of ~ 3 mm, for temperature excursions of ± 50° C (± 90° F). If required, partial correction for these excursions could probably be made using epoch and climatic data together with an appropriate thermo-mechanical model for support structure deformations.

As explained in §3 and §4, velocity aberration correction is achieved by designing the RR far-field diffraction patterns to exhibit a symmetrical *twin-lobe* structure. Each of the RRs must be oriented (about its local normal) in a particular direction with respect to the overhead spacecraft tracks, in order to achieve appropriate alignment of the reflected lobes.

Although a 45° inclination of the peripheral reflectors provides good overall FOV coverage and has been assumed in the following analyses, the choice of this value is somewhat arbitrary. Parametric analysis could reveal a more favourable inclination, depending on the criteria used to trade link budget performance at high zenith-angles against FOV overlap limitations. Variants involving more than 4 peripheral reflectors could also be considered, although they would incur an increase in the extent of FOV overlap, and higher overall GT costs.

It is assumed that the spacecraft (S/C) ranging strategy will inhibit operation for the small percentage of geometries where crosstalk effects are expected to be strong and determines, for any *allowed* ranging operation, which of the RRs must be providing the return signal. An appropriate deterministic correction then relates the measured RR range to a common GT reference point.

3. PRINCIPAL INFLUENCES IN LINK BUDGET PERFORMANCE

As shown in Fig.2, there several quite different influences which can affect the system link budget performance. Those which are considered or referred to in the present paper are listed below :

- Two-way atmospheric transmission, depending on visibility conditions, local zenith angle and GT altitude.
- Atmospheric turbulence, characterised by wavelength and the mean *long*-exposure turbulent energy ($\int C_n^2\ (h).dh$).
- Ranging geometry, as determined by local zenith angle, local RR incidence angle, satellite azimuth and range.
- Velocity aberration, depending on ranging geometry and satellite height and velocity.
- Retroreflector characteristics such as size, optical quality and dihedral angle spoiling.
- Detection techniques, which in the case of GLRS-R imply the use of a receiving telescope, transfer optics and a streak camera.

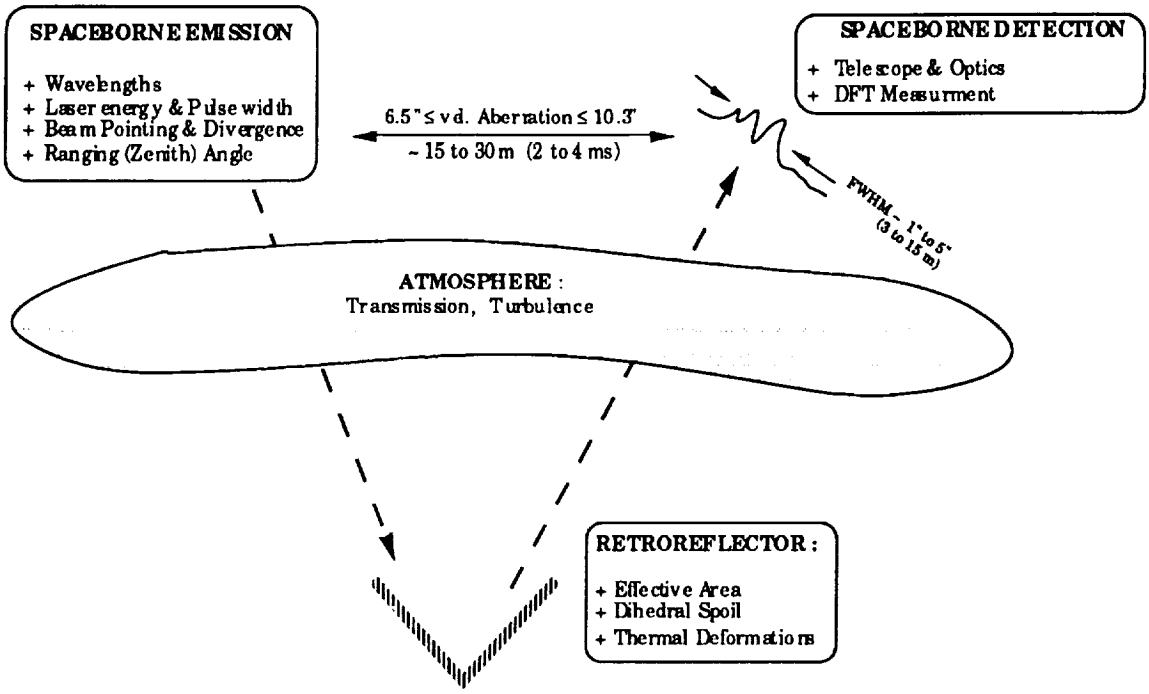

Figure 2. Factors contributing to link-budget performance

The schematic depicts an emitted (laser) beam of given wavelength, energy, pulse width and divergence which, on traversing the earth's atmosphere, is attenuated and degraded in wavefront uniformity. The RR returns the incident beam, introducing *vignetting* (defined by the intersected aperture and local incidence angle), additional *thermal* (and/or *manufacturing*) wavefront perturbations, a certain degree of *energy loss* (due to the reflectivity of the RR mirror surfaces) and a small *point-ahead* correction (by virtue of the dihedral angle spoil). The point-ahead is designed to compensate for the angular displacement of the S/C during the return propagation time of the emitted pulse. Having once *again* traversed the turbulent atmosphere, the reflected wavefront diffracts into space to form a resulting *speckle* pattern (characterised by the path-integrated turbulence strength). The mean received energy at the ranging telescope can be related to the mean *spread* of the speckle pattern and to the *pointing residual* - defined as the angular *difference* between the spacecraft and nominal reflected beam directions at the instant of pulse return.

The accuracy of the resulting range determination depends not only on the respective numbers of collected photons (at the doubled and tripled Nd:YAG wavelengths - 355 & 532 nm), but also on the implemented detection and signal processing techniques. Although these GLRS-R design features are not presented in greater detail here, they are implicitly included in the range accuracy calculations presented in § 9.

4. POINT-AHEAD CORRECTION OF VELOCITY ABERRATION

As shown in the above figure, at the GLRS-R orbit the S/C is displaced by an angular distance ranging between 6.5 and 10.3 arcseconds (equivalent to ~ 15 - 30 m) during the 2-way propagation time. The FWHM of the return beam is however, for a 100 mm RR, of the order of 1 to 5 arcseconds. The ambition of the point-ahead correction is thus to compensate as well as possible for this effect.

Fig. 3 illustrates the approach used in the GLRS-R GT concept, in order to achieve acceptable velocity aberration correction by means of a small degree of point-ahead applied to the retroreflected beams. Both diagrams are scaled in arcseconds as viewed from the RR, with the center corresponding to the direction of any given incoming beam. The central spot would thus also correspond to the required *return* beam direction if the S/C had no transverse velocty with respect to the RR.

The left-hand diagram illustrates (relative to the origin defined at the instant of pulse emission) the angular loci of the S/C at the instant of pulse *arrival* back at the S/C. The amplitude of any particular locus is commonly referred to as *velocity aberration*. The size and shape of these loci depend on the transverse (relative to the instantaneous line of sight) vectorial components of S/C velocity, within the foreseen limits of ranging geometry. The presence of two loci subsets results from the approximately opposite directions in which the S/C can move, as observed from the ground (i.e for *ascending* or *descending* tracks). These regions change and increase in size at increasing GT latitudes, in accordance with the wider range of directions of apparent S/C trajectory.

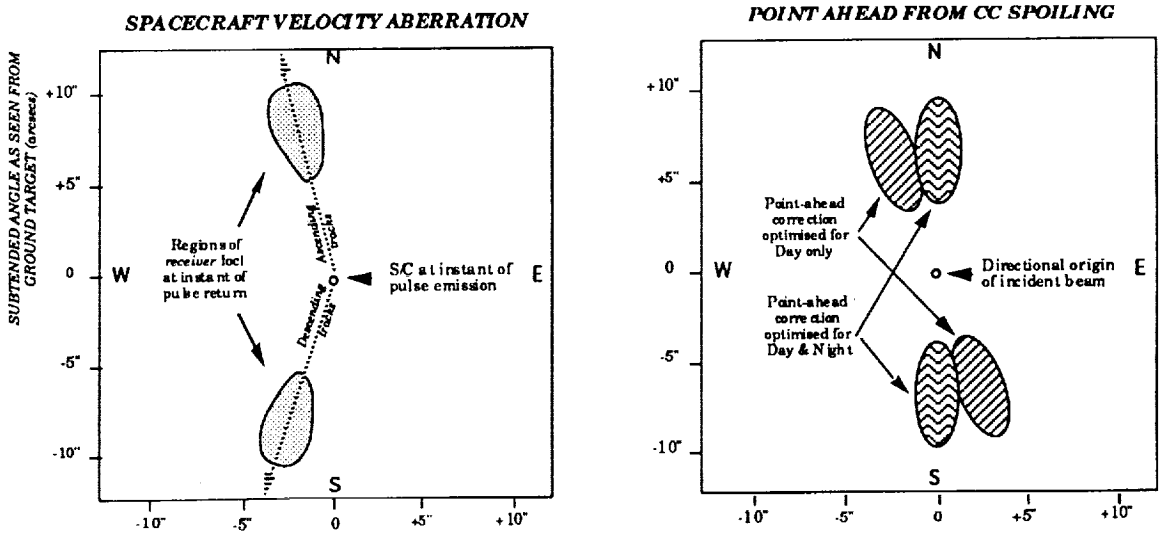

Figure 3. Point-ahead correction of velocity aberration.

The right-hand diagram illustrates how the RR point-ahead "attempts" to compensate for velocity aberration, by generating two return beams, offset in equal and opposite directions with respect to the incoming beam. The wavefront fold is achieved by what is commonly referred to as "dihedral angle spoiling", whereby one (or more) of the 3 RR dihedral angles is offset from the nominal value of 90.000°. Spoiling of a single angle leads to 2 reflected beams, whereas uniform spoiling of all 3 angles will (as is the case for most geodetic satellite reflectors) generate 6 evenly distributed return beams. The exact shape of the retroreflected directional loci is a geometrical consequence of the local incidence angles of the incoming beam with respect to the cube-corner retroreflector and to the orientation of its spoiled dihedral angle(s). The inclination of the two loci shown here can be modified in order to optimise the return signal strength during either *day* (ascending) or *night* (descending) S/C tracks. An alternative solution, as illustrated in Fig.3, would be to incline the RR so as to achieve a compromise compensation for both day and night tracks.

The degree to which velocity aberration is adequately compensated for, at a given ranging geometry, is referred to here as the beam *pointing residual*. It is expressed, in arcseconds, as the difference between the *required* (velocity aberration) direction and the *applied* (point-ahead) direction. In general, the smaller the domain of ranging geometries for which the RR point-ahead compensation is designed, the smaller the mean value of pointing residual.

Other factors influencing this mean performance are local RR incidence angle and orientation, GT lattitude, and the choice between day (or night)-only and day+night E/R track compensation.

5. GLRS-R GROUND TARGET OPTIMISATION AND PERFORMANCE

In the following link budget analyses, the GT performance is expressed in terms of *cross-section* profiles, which are derived take into account the appropriately computed *pointing residuals*. Although other performance criteria could have been chosen, these tend to be more difficult to characterise with a single curve, as they can depend on extrinsic influences such as turbulence and wavelength.

Fig. 4 illustrates, for the required GLRS ranging geometries, the variation in optimal values of dihedral spoil angle as a function of GT latitude and RR orientation. The optimisation process is designed to determine (for a given GT, S/C and latitude characteristics) the dihedral spoil which minimises the quadratic sum of pointing residuals.

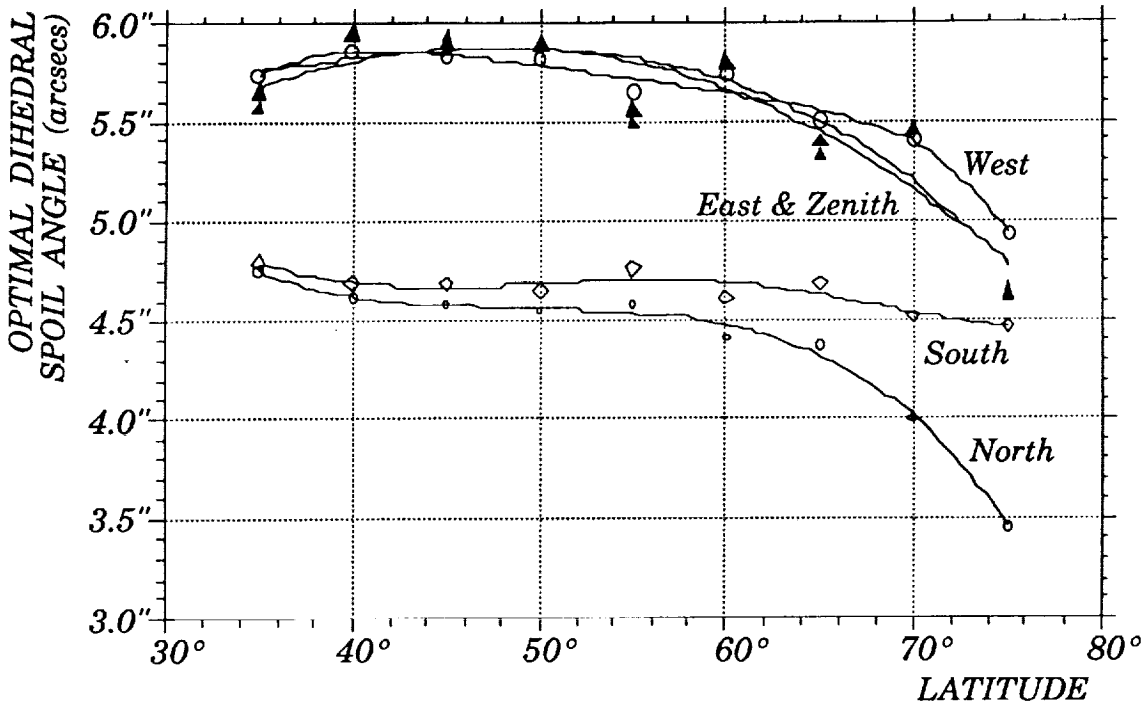

Figure 4. Optimal dihedral angle spoil as a function of latitude.

The curves shown here correspond to the nominal GLRS orbit and to a day/night optimisation of the pointing residuals. The following two figures illustrate the expected GT performance at a GT latitude of 35°, in terms of optical *cross-section*. The choice of this quantity is partly due to its similarity to the familiar notion of radar cross-section, and partly to its physical significance; the RR cross-section can be thought of as the equivalent surface area of a perfectly white (albedo = 1) Lambertian diffuser. Such a diffuser, if exposed to a uniform illumination equal in intensity to that intersected by its equivalent retroreflector, would give rise to the same far-field luminous flux as that produced by the retroreflector in the considered point-ahead direction. For a perfect RR, on-axis and in the absence of turbulence, the theoretical cross-section can be shown (for a 2-lobe diffraction pattern) to be :

$$\zeta = (\pi^3/16).(\phi^4/\lambda^2) \sim 1500.\ 10^6\ m^2$$ (~ 100 x greater than in Fig.5)

In practice, the RR is rarely ranged to directly on-axis, and atmospheric turbulence induces considerable beam-spread. A certain degree of spreading is in fact desireable since the retroreflected beam would otherwise be extremely narrow (~1 arcsec in the above example), with a consequently dramatic fall-off in received energy at pointing residuals beyond about 2 arcsecs.

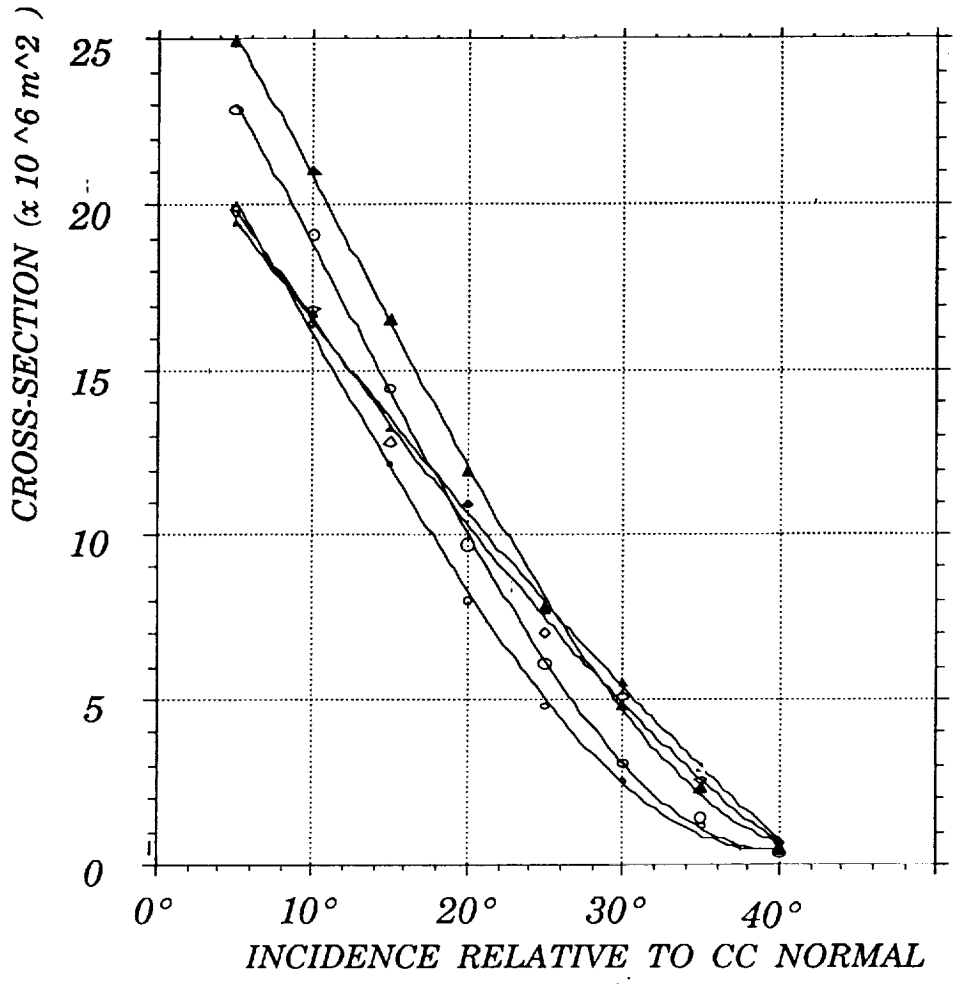

Figure 5. Mean cross-section profiles vs. local incidence angle

The variation of cross-section profile, as shown here, is given as a function of local incidence angle and CC orientation, for a "moderate" degree of turbulence (see also § 7) and at λ = 532 nm. The disparities in cross-section profile, from one RR orientation to another, can be largely explained by differences in the range of velocity aberration vectors to be corrected for within each individual FOV.

For most purposes, the fall-off in CC cross-section with increasing incidence angle can be adequately approximated by a straight line with 40° zero-crossing. This fall-off is nevertheless a factor of considerable importance when considering the global GT performance; the most probable CC incidence angle is that of least mean cross-section.

6. THE CHOICE BETWEEN DAY AND NIGHT TRACK OPTIMISATION

In the GT design process, the choice can be made between a preference for ranging during one only (Day/Night) or both (Day and Night) of the S/C tracks (see also Fig. 3). The corresponding point-ahead corrections are then computed to provide the least overall pointing residuals.

In Fig. 6 the expected mean variations of RR cross-section are traced for the above 2 cases, and for the unfavourable case of ranging at *night* (*day*) to a *day* (*night*) -optimised GT. It can be seen that the latter case gives rise to a considerable degradation in mean cross-section. Alternatively, a good compromise can be achieved between day and night optimisations, as shown by the curve with full triangles. Such an approach has the advantage that it does not restrict the ranging opportunities to just half of the S/C overhead tracks.

It could also be argued that night-time turbulence is in general much lower than that encountered under hot daytime conditions, thus compensating for the potential disadvantage of ranging at night to a *day*-optimised GT.

For any given GT location, the choice of track optimisation could forseeably be made, in accordance with an amalgum of site-specific parameters, so as to enhance the global probability of accurate range measurements.

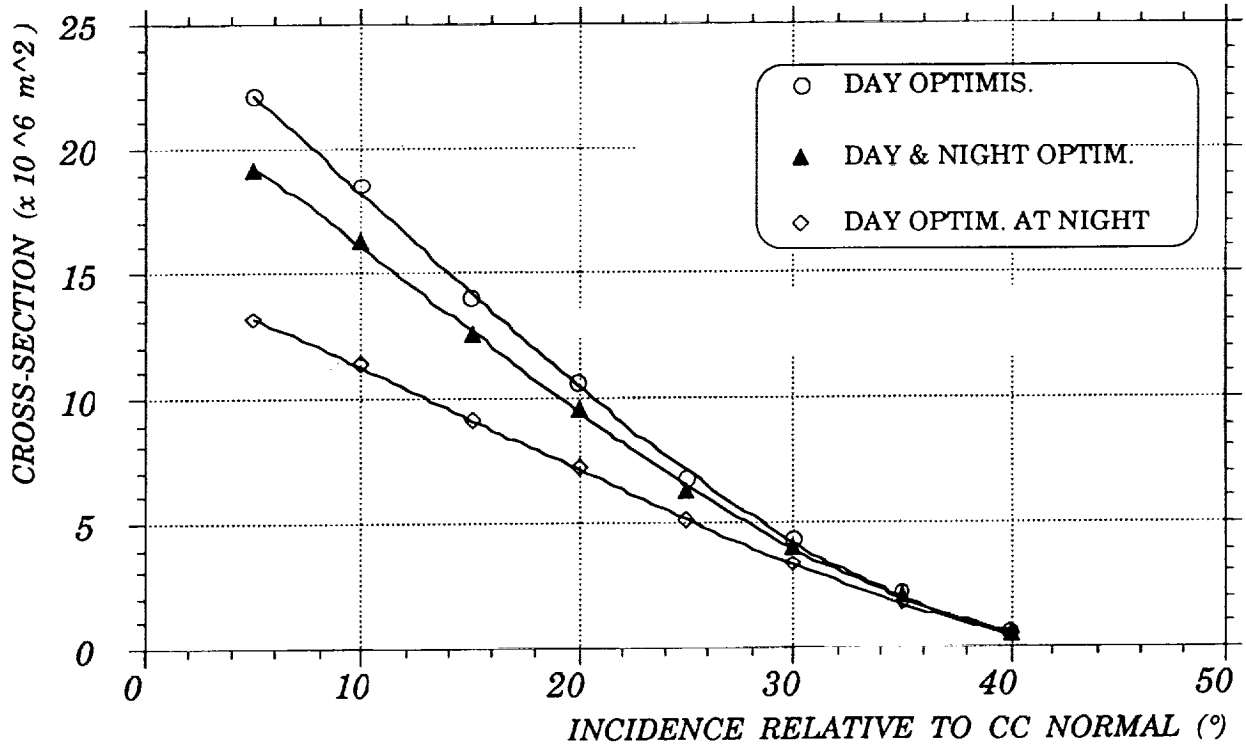

Figure 6. Mean peripheral retroreflector cross-section vs. track optimisation.

7. INFLUENCE OF ATMOSPHERIC TURBULENCE ON GT PERFORMANCE

The role of turbulence in the GLRS-R link budget performance is of considerable importance, as it can introduce strong changes to the overall system performance.

In Fig. 7, the expected mean peripheral cross-section profiles are traced for 3 values of atmospheric turbulence strength, considered to represent (respectively) low, moderate and high levels of turbulence; 10, 50 & 100 x 10^{-13} $m^{1/3}$. Good night-time conditions might correspond to the "low" level, whereas high temperature daytime conditions could generate even worse turbulence than that assumed under "high" conditions.

The unit of turbulence strength used here is that of refractive index structure (or turbulent energy) integral :

$$\int C_n^2 \, (h) \, . \, dh \quad (m^{1/3})$$

The choice of this quantity, rather than Fried's parameter r_o or *Seeing*, has been made because of its independance from wavelength. Table 1 provides conversions between these units, for a few selected values of extreme and typical turbulence integral.

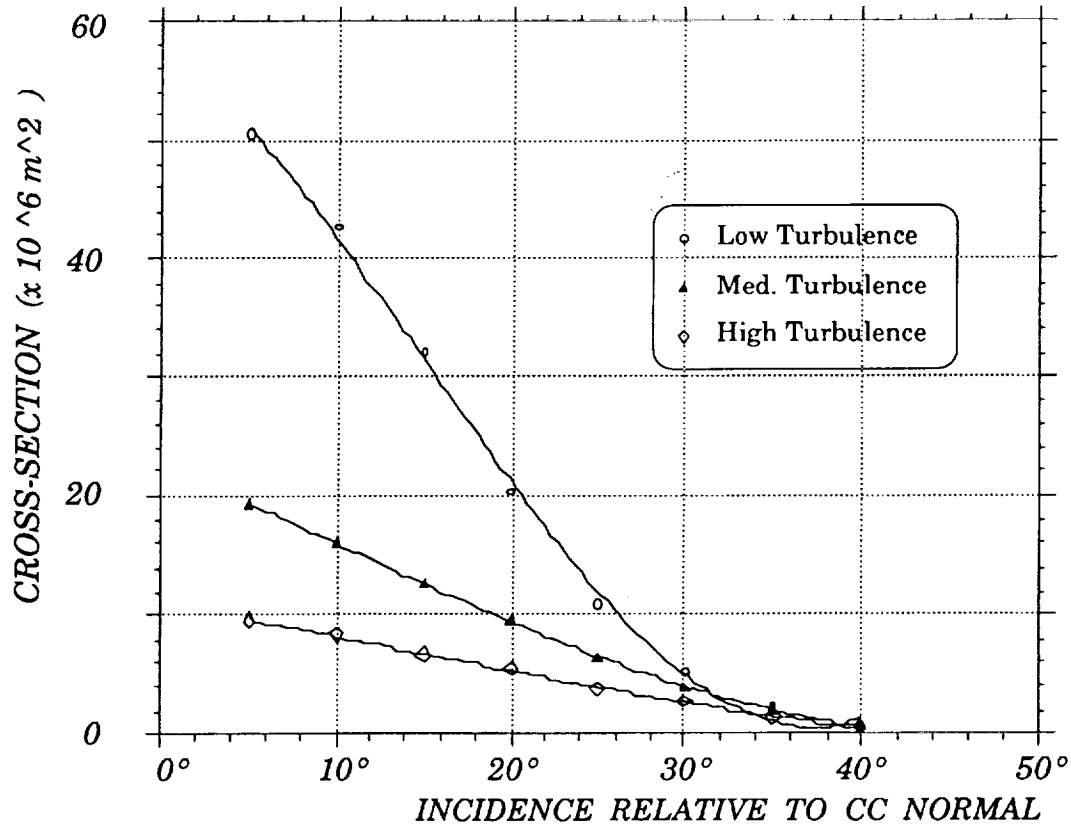

Figure 7. Variation of mean peripheral cross-section as a function of turbulence.

$\int C_n^2$ (h) .dh (m 1/3)	r_o (355 nm) (cm)	r_o (532 nm) (cm)	Seeing (355nm) (arcsec)	Seeing (532nm) (arcsec)
1. 10^{-13}	21.	34.	0.35	0.32
5. 10^{-13}	8.	13.	0.92	0.85
10. 10^{-13}	5.3	8.6	1.4	1.3
50. 10^{-13}	2.0	3.3	3.7	3.4
100. 10^{-13}	1.3	2.1	5.6	5.2

TABLE 1. Fried's parameter r_0 and seeing as a function of turbulent energy integral $\int C_n^2(h)$. dh.

As can be seen in Fig. 7, strong atmospheric turbulence can give rise to a considerable drop in the overall cross-section performance of the GT retroreflectors due to overspreading of the reflected diffraction patterns.

8. CROSSTALK EFFECTS AND SYSTEMATIC BIAS

The 3D plot shown in Fig. 8 illustrates the notion of inter-RR crosstalk, expressed in terms of range measurement bias, which results from the detection of retroreflected energy originating from more than one RR.

The bias is determined at the level of the Streak Camera differential flight time measurement, where the (temporal) barycenters of the Green and UV return pulses are calculated. In the case of multiple returns, the Streak Camera detection algorithm can be confused by the presence of more than one pulse within the streak scan time-window (typically ~ 10 ns). Assuming the strongest pulse to be that of interest, the influence of a secondary echo is evaluated here in terms of the (distance) bias it would introduce into the timing determination.

The four crosstalk zones, generated by peripheral FOV overlap, correspond in fact to ranging geometries of reduced interest because of the weak return signal strength to be expected at the edge of any of the RR's local FOV (see 3 previous charts). In the bias zones corresponding to overlap between the zenith RR and any of the peripheral RRs, either one of the two following strategies would need to be applied :

1 The GLRS system ranging controller software would forbid ranging at this limited set of geometries.

2 The detection data processing would be designed to account for the deterministic bias effects, giving preference to the range determination based uniquely on the (clearly strongest) pulse returns originating from the nearest RR.

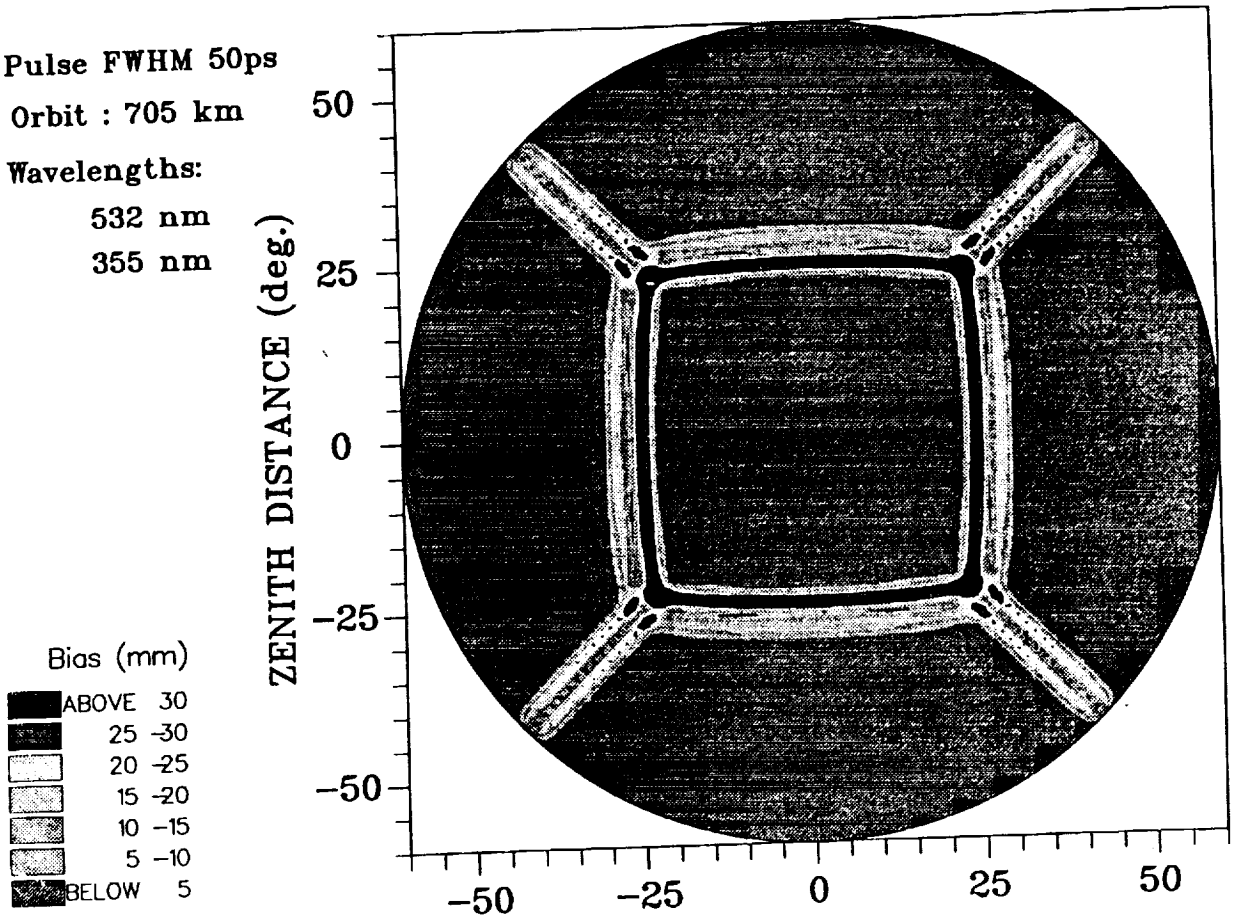

Figure 8. Systematic bias related to multiple pulse returns arising from FOV overlap.

9. LINK BUDGET CALCULATIONS AND EXPECTED RANGE ACCURACY

Although the GT performance has been expressed, in Figs. 5 - 7, in terms of cross-section, these figures need to be translated into photons in order to assess the system range measurement performance. The correspondance between these 2 quantities depends on the following factors :

- Emitted pulse wavelength, energy and beam divergence.
- Two-way atmospheric transmission at the given range angle **Z**.
- Emitter - GT - receiver range (also a function of **Z**).
- Receiving telescope diameter.
- Miscellaneous optical component efficiencies.

The curves shown in Fig. 9 express the expected numbers of received photons at the GLRS detector as a function of **Z**, at the least transmitted (355 nm) wavelength, for two values (*5km* and *23km*) of standard atmospheric visibility and selected values of cross-section. It can be seen that at high zenith angles there is a sharp drop in received energy and a widening gap between the 5 and 23 km performances.

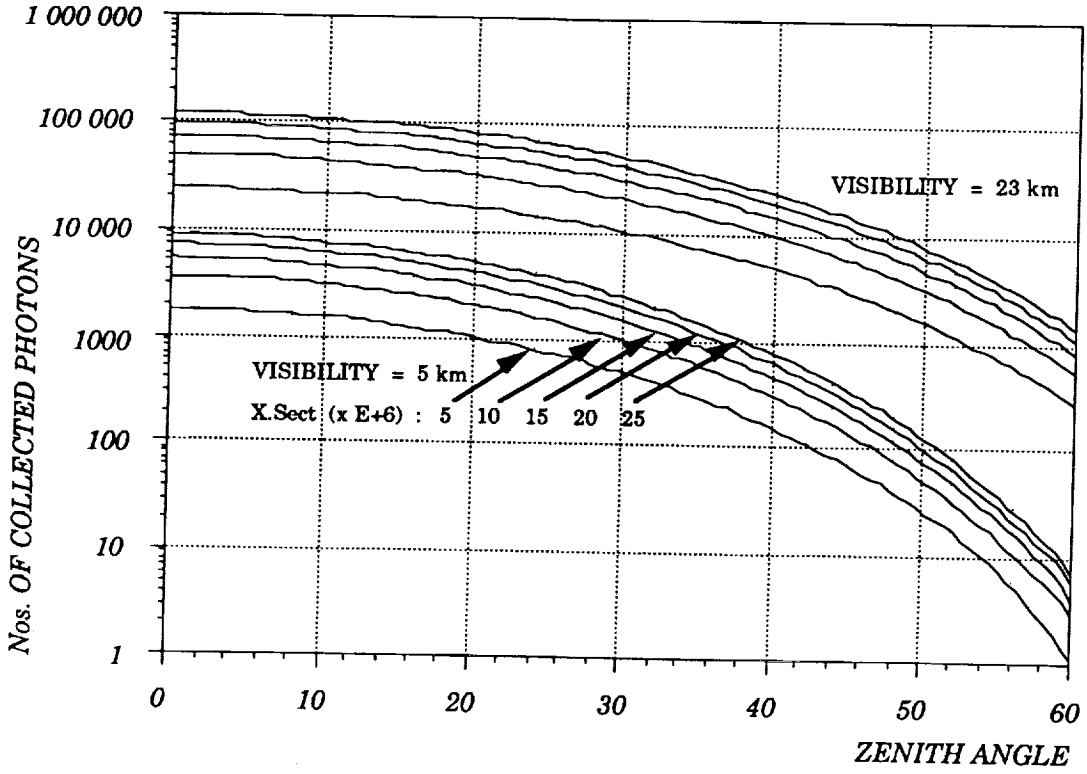

Figure 9. Received photons @ 355nm as a function of zenith angle, visibility and cross-section.

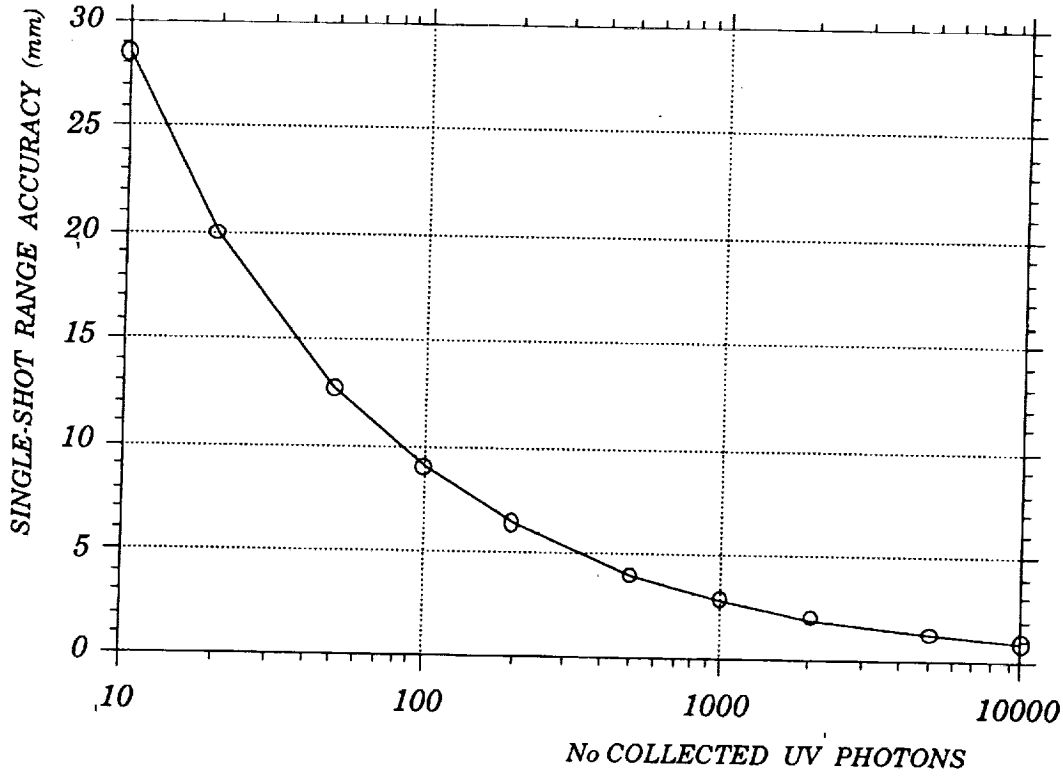

Figure 10. Range accuracy as a function of collected uv photons.

10. INFLUENCE OF THERMAL EXTREMES ON DIFFRACTION PATTERNS

In all of the preceeding analyses, atmospheric turbulence has been the only influence considered in terms of a potential source of wavefront deformation. However, thermal distortions of the RR itself, under conditions of extreme ambient temperature or midday solar illumination, could also be expected to introduce some degree of change into the retroreflected beams. These effects have been simulated firstly by running Nastran finite element simulations of the structural distortions of an assumed mechanical RR design. The resulting deformations of the reflecting surfaces were then introduced into the optical code used to generate retroreflected wavefronts and their corresponding far-field diffraction patterns.

The diffraction pattern shown in Fig. 11 has been derived from the simulated conditions of low ambient air temperature (-15°C) in the absence of solar illumination (midnight), and shows that there is indeed some spreading of the return beams. Various other simulations have also been run, and show that extreme heat can also have a detrimental effect on the retroreflected beam quality. These simulations are of course highly (thermo-mechanical) model dependant, but nevertheless show that under conditions of moderate ambient temperature (-5° to +25°C) there is no significant degradation of the diffaction lobes.

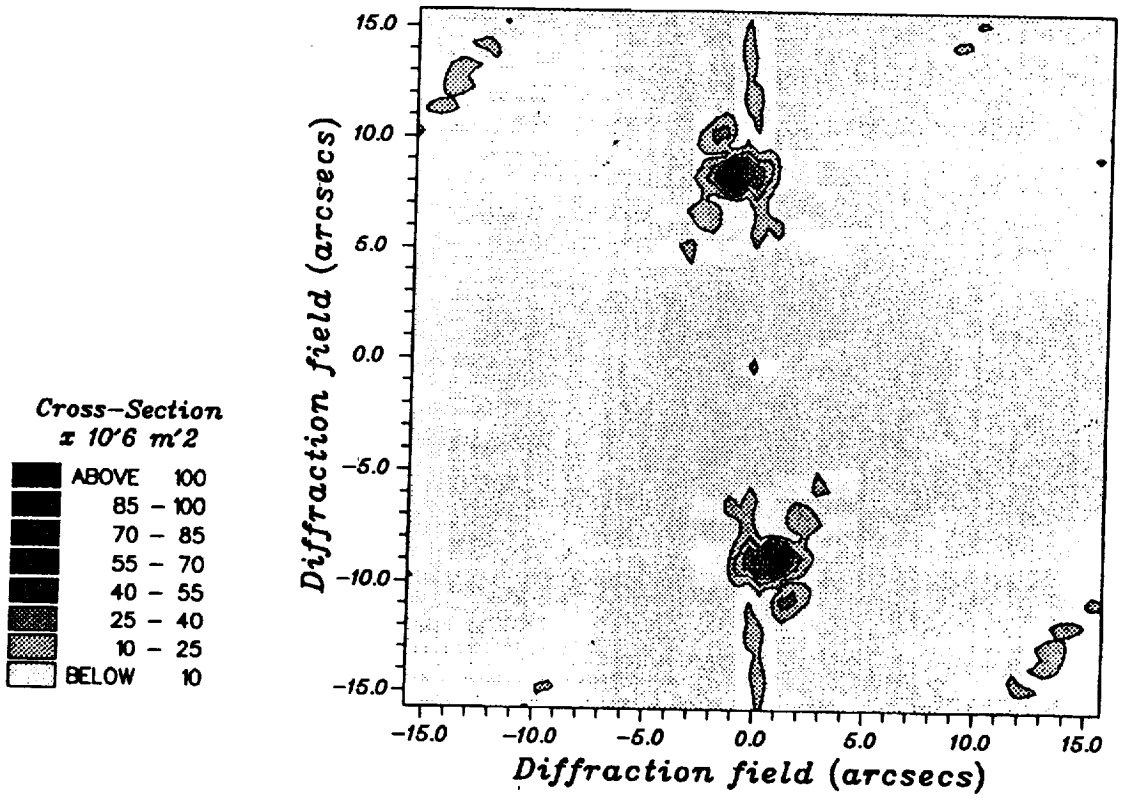

Figure 11. Simulated GLRS diffraction lobe distortion at -15°C.

11. CONCLUSIONS

The GLRS-R Ground Target design approach and analyses described in the present paper are found to satisfy the system requirements under most ranging conditions, as summarised by the following points:

- A relatively small number of retroreflectors can satisfactorily cover the observable sky up to zenith angles of 60°.
- Minimal zones of undesireable crosstalk are achieved.
- Appropriate spoiling of the retroreflectors can enable good correction of velocity aberration to be assured while maintaining high return signal strength at most rangiong geometries.
- Just 2 values of dihedral spoil angle are needed for most practical latitudes, thus leading to considerable simplification of their manufacture, assembly and testing.
- The Ground Target performance is found to have a minimal dependance on site location, for latitudes up to 65° (north or south).
- The system performance is quite strongly dependant on atmospheric turbulence.
- Thermal influences can become non-negligeable under extreme ambient temperature conditions.
- The overall link budget performance is found to be such that under typical conditions, a single-shot ranging accuracy of 1 cm or better can be expected.